



New route to toxic nitro and nitroso products upon irradiation of micropollutants mixtures containing imidacloprid: role of NO_x and effect of natural organic matter

Davide Palma, Yara Arbid, Mohamad Sleiman, Pascal de Sainte-Claire, Claire Richard

► To cite this version:

Davide Palma, Yara Arbid, Mohamad Sleiman, Pascal de Sainte-Claire, Claire Richard. New route to toxic nitro and nitroso products upon irradiation of micropollutants mixtures containing imidacloprid: role of NO_x and effect of natural organic matter. *Environmental Science and Technology*, 2020, 54, pp.3325-3333. hal-02524858

HAL Id: hal-02524858

<https://hal.science/hal-02524858>

Submitted on 30 Mar 2020

HAL is a multi-disciplinary open access archive for the deposit and dissemination of scientific research documents, whether they are published or not. The documents may come from teaching and research institutions in France or abroad, or from public or private research centers.

L'archive ouverte pluridisciplinaire **HAL**, est destinée au dépôt et à la diffusion de documents scientifiques de niveau recherche, publiés ou non, émanant des établissements d'enseignement et de recherche français ou étrangers, des laboratoires publics ou privés.

**New route to toxic nitro and nitroso products upon irradiation of micropollutants
mixtures containing imidacloprid: role of NO_x and effect of natural organic matter**

Davide Palma, Yara Arbid, Mohamad Sleiman*, Pascal de Sainte-Claire, Claire Richard*

Université Clermont Auvergne, CNRS, SIGMA Clermont, Institut de Chimie de Clermont-
Ferrand, F-63000 Clermont-Ferrand, France

* : Corresponding authors :

Mohamad.sleiman@sigma-clermont.fr and Claire.richard@uca.fr

Tel : +33 (0)4 73 40 71 42

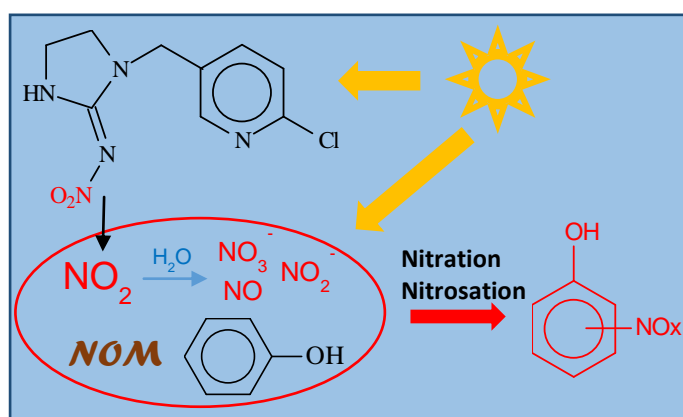
Fax : +33 (0)4 73 40 77 00

ABSTRACT

In this study we reveal the capacity of imidacloprid (a neonicotinoid insecticide) to photoinduce nitration and nitrosation of three aromatic probes (phenol, resorcinol, tryptophan) in water. Using a gas-flow reactor and NO_x analyzer, the production of gaseous NO/NO₂ was demonstrated during irradiation (300-450 nm) of imidacloprid (10⁻⁴ M). Quantum calculations showed that formation of NO_x proceeds via homolytic cleavage of the RN-NO₂ bond in the triplet state. In addition to gaseous NO/NO₂, nitrite and nitrate were also detected in water, with the following mass balance: 40±8% for NO₂, 2±0.5% for NO, 52±5% for NO₃⁻ and 16±2% for NO₂⁻. The formation of nitro/nitroso probe derivatives was evidenced by high resolution mass spectrometry and their yields were found to be ranging between 0.08% and 5.1%. The contribution of NO₃⁻/NO₂⁻ to the nitration and nitrosation processes was found minor under our experimental conditions. In contrast, the addition of natural organic matter (NOM) enhanced significantly the yields of nitro/nitroso derivatives, likely via production of

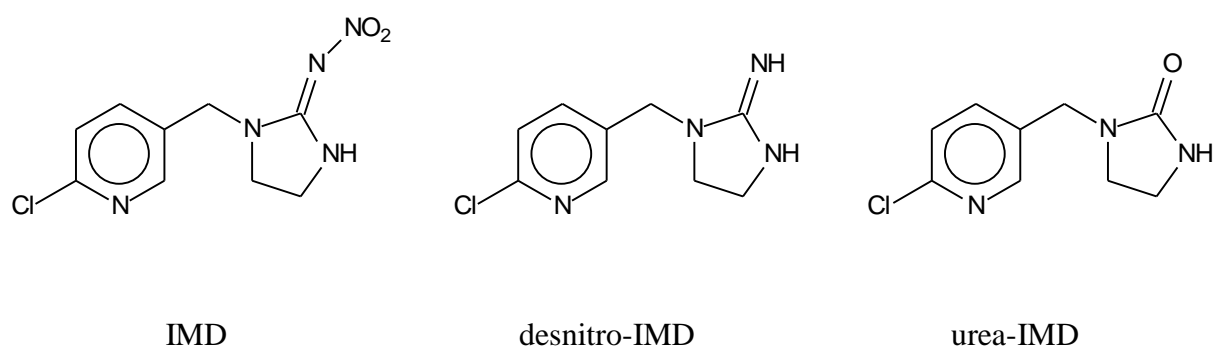
19 triplet excited states ($^3\text{NOM}^*$) and HO^\cdot . These findings reveal the importance of investigating
20 the photochemical reactivity of water contaminants in mixture to better understand the
21 cocktail effects on their fate and toxicity.

22 Graphical abstract



INTRODUCTION

Imidacloprid (1-[(6-chloropyridin-3-yl)methyl]-N-nitro-imidazolidin-2-imine, IMD, Scheme 1) is a widely used and effective neonicotinoid insecticide.¹ IMD, like other neonicotinoids, is used in a variety of crops and its applications have been recently extended to domestic sector and animal health.¹ Once released in the environment, it can reach the aquatic, atmospheric and terrestrial compartments and be in contact with a lot of living organisms.²⁻⁴ IMD affects the central nervous system of insects⁵ and there are increasing concerns about its deleterious effects with confirmed toxicity for pollinators, especially bees.⁶ Toxicity or adverse effects in other species has been also reported⁷⁻⁹.



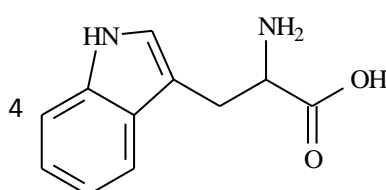
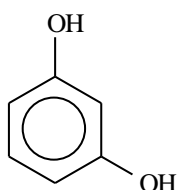
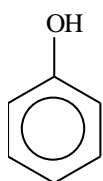
Scheme 1: Molecular structure of IMD and its main photoproducts

Several studies have been performed to investigate the fate of IMD under solar light, mainly in aqueous solutions^{1, 10-13} on plant leaves and cuticles¹⁴⁻¹⁶ and more recently on solid thin films¹⁷. Desnitro -IMD (1-[(6-chloropyridin-3-yl)methyl]imidazolidin-2-imine) was reported to be the main photoproduct and the urea-IMD (1-[(6-chloropyridin-3-yl)methyl]imidazolidin-2-one), a minor photoproduct (Scheme 1).¹⁶ The formation of these by-products seems to imply the cleavage of the N-NO₂ bond; however, the fate of NO₂ is not yet clear. Recently, the formation of gaseous nitrogen oxides during the irradiation of IMD at the surface of a germanium attenuated total reflectance (ATR) crystal was investigated.¹⁷ The

41 authors detected nitrous oxide (N_2O) which was proposed to be formed by recombination of
42 detached NO_2 with the IMD fragments in the electronic ground state.

43 In previous studies, we showed that the fungicides chlorothalonil and thiophanate-methyl can
44 photoinduce the degradation of other pesticides during irradiation.^{18,19} These reactions can
45 take place in surface waters where fungicides are present together with a wide range of other
46 chemicals and on solid supports such as the surface of leaves where pesticides are often
47 applied in combination. However, the effect that a pollutant can have on another pollutant
48 remains largely overlooked in photochemical studies and little is known on the transformation
49 of photostable pollutants *via* light induced reactive intermediates of other co-pollutants. The
50 ability of IMD to release NO_2 upon irradiation makes this compound important to study in
51 this context since nitration of chemicals have been reported in a lot of systems generating NO_2
52 ²⁰⁻²⁸.

53 The goal of this study was thus to explore the formation of reactive NO_x *via* IMD photolysis
54 and their reactivity towards surrogates of water contaminants and typical moieties of natural
55 organic matter (phenol, resorcinol and tryptophan). In particular, we investigated the
56 formation of nitro and nitroso-derivatives, two potentially toxic categories of compounds,
57 from the three selected probes under polychromatic irradiation (300-450 nm) in the presence
58 of IMD. Experiments were carried out using a flow-tube reactor equipped with NO_x analyzer
59 whereas the formation of by-products was characterized using high resolution UHPLC-ESI-
60 MS. Theoretical calculations were also performed to elucidate the mechanisms of NO_x
61 formation. To the best of our knowledge, this is the first study reporting on the measurement
62 of NO_x during irradiation of IMD in water and on their role in nitrosation/nitration of other
63 water pollutants. Environmental implications of this light-induced indirect degradation are
64 discussed.



phenol

resorcinol

tryptophan

65 **Scheme 2:** Selected probes

66 **MATERIALS AND METHODS**

67 **Chemicals and materials.** Imidacloprid (Pestanal[®], analytical standard), resorcinol (purity
68 99%), phenol (purity $\geq 99.5\%$), L-tryptophan (purity $\geq 98\%$) and 2,4-dinitrophenylhydrazine
69 (DNPH, purity 97%) were purchased from Sigma-Aldrich and used as received. Sodium
70 nitrite (Rectapur 98%), sodium nitrate (Fluka, purity 99%), 2 and 4-nitrophenol (Fluka, purity
71 $\geq 99\%$) and 4-nitrosophenol (Aldrich-Chemie, purity 60% due to a content of water of 40%)
72 were also used without further purification. Suwannee River NOM (2R101N) was purchased
73 from IHSS. Water was purified using a reverse osmosis RIOS 5 and Synergy (Millipore)
74 device (resistivity 18 M Ω cm, DOC < 0.1 mg.L⁻¹). All solvents or other reactants were of the
75 highest grade available.

76 **Irradiations.** Two different irradiation devices were used. To monitor NO_x formation in the
77 gas phase, device 1, was designed with a cylindrical Pyrex gas flow-reactor (0.65 L, length 27
78 cm and diameter 5.7 cm) containing 200 mL of IMD solution (10⁻⁴ M or 25.6 mg.L⁻¹) and
79 irradiated from the top with two fluorescent tubes (Sylvania F15W/BL 368, 438 mm×26 mm,
80 300-450 nm, λ_{max} at 365 nm, see Figure SI-1) placed at a distance of 5 cm. The rate of
81 incident light entering the solution was measured using a QE65000 (Ocean optics) radiometer, it
82 was equal to 1.3×10¹⁶ Photon.cm⁻².s⁻¹. The gas flow-reactor was connected to a NO_x
83 chemiluminescence analyzer (Thermo Scientific i-42 NO_x analyzer) as shown in Figure 1.
84 Experiments were carried out under continuous flow of clean air, to reduce the residence time
85 of NO_x and minimize NO₂ photolysis. Gaseous inlet of the reactor was connected to flow

86 controllers for N₂ and O₂ (model Brooks 4800 series) allowing to select the atmosphere under
87 which the irradiations were performed (pure N₂, pure O₂ or a 80/20 O₂/N₂ mixture) and to
88 adjust the flow rate to 0.7 L min⁻¹. Background levels of NO_x in the gas inlet were negligible
89 (<0.4 ppbv). Before irradiation, the levels of NO_x in the gas phase of the reactor were
90 monitored continuously every 10 seconds until reaching a steady state within few minutes
91 (Figure SI-2). Despite that NO₂ concentrations up to 40 ppbv were detected initially (first
92 30s), a background level of NO_x (<5 ppbv) was quickly reached. This production of NO₂
93 might possibly be due to IMD photolysis under indoor lighting during preparation and
94 handling of the solutions. During IMD irradiation, we have chosen to monitor NO_x levels in
95 the gas phase of the reactor at selected times and not continuously. After selected irradiation
96 times, the light was turned off and the outlet of the reactor connected to the NO_x analyzer.
97 NO_x were measured every 10 s for a period of 1-2 min at a flow rate of 0.7 L min⁻¹. The time
98 profile of NO_x concentrations shown in Figure SI-2 corresponds to the decay of NO_x level in
99 the reactor due to the dilution with clean air. The level of NO_x measured was relatively
100 constant at 1h, 2h, 4h and 6h of IMD irradiation, in accordance with a steady state regime.
101 The levels of NO_x generated were then obtained by integrating the time profiles of NO_x
102 concentrations. For calculating the yields of NO_x, the ratio of NO_x concentrations (ppbv)
103 were converted into molar by taking into account the gas phase volume of the reactor (450
104 mL). By measuring the converted quantity (in moles) of IMD during the irradiation period, it
105 was possible to calculate the molar yield for NO and NO₂.

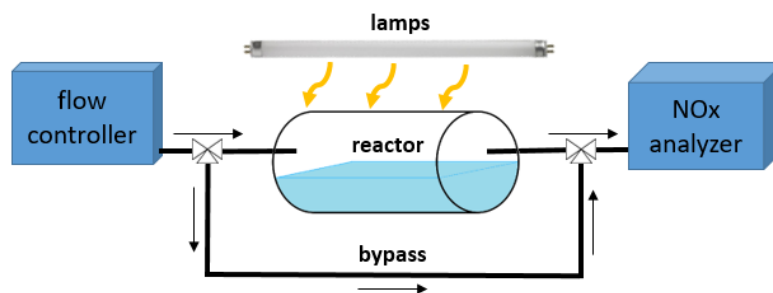


Figure 1. Schematic representation of device 1 used to monitor NO_x formation upon irradiation of IMD solutions.

A second device, device 2, was used to monitor the formation of nitro and nitroso-derivatives. 15 mL of solutions were placed in a cylindrical Pyrex reactor sealed with an air-tight silicon cap and surrounded by six fluorescent tubes (Sylvania F15W/BL 368), installed inside a custom-made cylindrical irradiation device. Solutions were not buffered, but pH was controlled during the reactions. The initial pH was 6.5 ± 0.3 and in the course of the reactions, pH laid above 5. In the case of IMD+resorcinol mixtures, aliquots were sampled after several selected irradiation times and the consumption profile of IMD and nitro- and nitroso-resorcinol were obtained. For IMD+phenol and IMD+tryptophane mixtures and experiments with nitrate/nitrite and NOM, aliquots were only sampled after 16 h of irradiation. Samples were analyzed by HPLC to monitor the loss of IMD and the probes and by UHPLC-HRMS to characterize photoproducts and estimate their levels. For the experiment at 10^{-5} M of IMD and 10^{-4} M of resorcinol, 75 ml were irradiated by portions of 25 ml, and water was evaporated up to 6 ml using a rotavapor before further analyses. Experiments were done in duplicate or triplicate. **Analytical methods.** Absorption spectra were recorded using a Varian Cary 3 spectrophotometer. IMD, phenol, resorcinol and L-tryptophan concentrations were monitored by HPLC (Waters Alliance 2695) equipped with a photodiode array detector (Waters 2996) and a EC150/4.6 Nucleodur 100-5 C₈ endcapped column. The HPLC conditions are presented in Table SI-1. was quantified using the same instrument after derivatization with DNPH.²⁹ 15

126 mL of derivatizing solution were prepared by mixing concentrated HCl, ultrapure water and
127 acetonitrile in the ratio 2:5:1. 50 μ L of this solution were added to 5 mL of sample solution.
128 Derivatization reaction was completed in 5 min and HPLC analyses were run shortly after.
129 Calibration used derivatized NO_2^- solutions in the concentration range 10^{-6} - 10^{-5} M. All the
130 HPLC analyses were done in triplicate and presented data are the mean values obtained.
131 NO_3^- was measured by ionic chromatography on a Dionex ICS-5000⁺ using a column model
132 Dionex Ion Pack AS11 2mm \times 250mm; the flow was 0.25 mL.min⁻¹ and the mobile phase was
133 an aqueous solution of KOH at the concentration of 0.43 mM for the first 4.5 min followed by
134 a linear gradient up to 18 min of runtime by rising KOH concentration up to 11.70 mM. The
135 injection volume was 750 μ L and the temperature of the column oven was set at 30°C.
136 External standards were prepared using NaNO_3 in the concentration range 50-200 μ g.L⁻¹.
137 Nitro and nitroso-derivatives of phenol, resorcinol and L-tryptophan were characterized and
138 their concentrations estimated by high resolution mass spectrometry (HRMS) performed on
139 an Orbitrap Q-Exactive (Thermo Scientific) coupled to an ultra-high performance liquid
140 chromatography system (UHPLC) Ultimate 3000 RSLC (Thermo Scientific). Due to the lack
141 available standards, desnitro-IMD and minor photoproducts were tentatively identified by
142 HRMS but quantification was not possible. Analyses were carried out both in negative (ESI^-)
143 and positive (ESI^+) electrospray modes. The column was the same column as for HPLC-UV.
144 The binary solvent system was composed of acetonitrile and acidified water using formic acid
145 at 40% and 60% respectively with a flow of 1.0 mL min⁻¹. Nitro and nitroso-phenols were
146 quantified by injection of external standards of 4-nitro and 4-nitroso-phenols at concentrations
147 varying from 5×10^{-7} to 4×10^{-6} M (Figure SI-3). Due to commercial unavailability of nitrated
148 derivatives, the concentrations of nitro and nitroso-resorcinols were estimated using the
149 calibration curves of 4-nitro and 4-nitroso-phenols. The concentrations of nitro-tryptophan
150 and nitroso-tryptophan were estimated using L-tryptophan at the concentration of 10^{-6} M as a

reference. Yields were obtained by dividing the photoproducts concentrations by the loss of IMD in concentration and by multiplying these ratios by 100.

Computational Method. Potential Energy Surfaces (PES) were investigated with the Gaussian series of programs.³⁰ Density Functional Theory (DFT) calculations (optimizations, frequency calculations, identification of transition states and IRC calculations) were performed at the MN12SX/6-311++G(d,p)//MN12SX/6-31+G(d,p) level of calculation. Among the large set of hybrid range-separated functionals that we tested, MN12SX³¹ gave the best agreement between experimental and theoretical absorption spectra. Finally, the time dependent-DFT (TD-DFT) method was used to compute singlet excited states. Triplet state was explored with conventional self-consistent field calculations. Solvent was modeled implicitly with the Polarizable Continuum Model (PCM). Electronic energies are reported throughout (Gibb's free energies are not provided here because low vibrational modes may introduce large uncertainties in this calculation).

RESULTS AND DISCUSSION

Photolysis of IMD. The degradation profile of neutral aqueous IMD (10^{-4} M) irradiated in device 1 is shown in Figure 2. HPLC-UV and UPLC-HRMS analyses indicated that the main photoproduct was desnitro-IMD (Figure SI-4). Three minor photoproducts were also found: a compound produced by addition of an oxygen atom on IMD (IMD+O), another one produced by addition of two oxygen atoms on desnitro-IMD (desnitro-IMD+2O) and the nitroso derivative of IMD (IMD-O) as traces (Table SI-2).

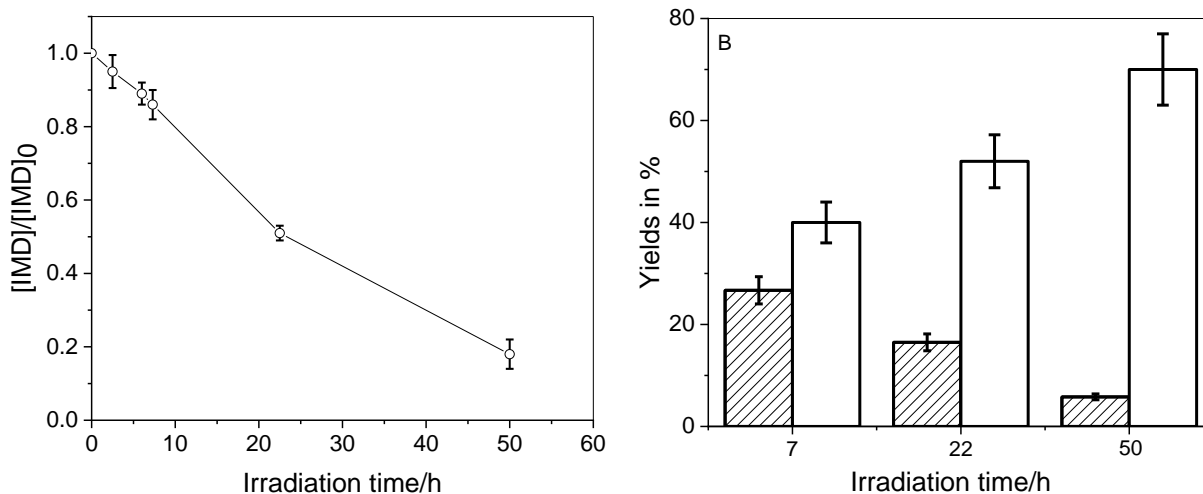
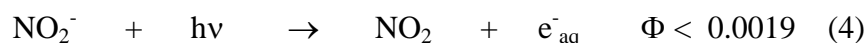
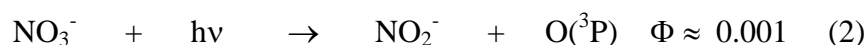
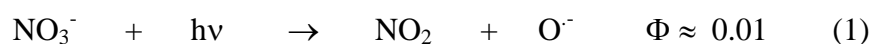


Figure 2. Consumption profile of aqueous IMD (10⁻⁴ M) irradiated in device 1 (A) and yields of NO₃⁻ (white bars) and NO₂⁻ (shaded bars) (B). Error bars are standard deviations.

NO₃⁻ and NO₂⁻ were detected in the aqueous phase (Figure SI-4). The yield of NO₃⁻ increased constantly to reach 72±5% after 50 h of irradiation (Figure 2B, white bars). In contrast, the yield of NO₂⁻ decreased from 27% after 7 h of irradiation to 6% after 50 h (Figure 2B, shaded bars). The higher accumulation of NO₃⁻ compared to that of NO₂⁻ is consistent with the spectral properties and the known photoreactivity of these ions. NO₃⁻ (λ_{max}= 300 nm and ε= 8 M⁻¹.cm⁻¹) absorbs much less solar light than NO₂⁻ (λ_{max}= 355 nm and ε= 22 M⁻¹.cm⁻¹) and its quantum yield of photolysis is also lower (reactions 1-4) leading to a smaller photolysis rate³²:



The detection of IMD+O and of desnitro-IMD+2O appear to be consistent with the formation of hydroxyl radicals through reactions (1) and (3).

NO_x formation upon irradiation of IMD. We also measured the NO_x formation in the gaseous phase above the solutions. NO and NO₂ were successfully detected upon irradiation of IMD (10⁻⁴ M) in device 1. Examples of collected data are shown in Figure SI-2. During the first two hours of reaction of irradiation, 24 µg of NO₂ and 0.88 µg of NO were produced whereas IMD loss was around 380 µg (See Table 2). After integrating nitrite and nitrate levels produced and considering the volume of gas (200 mL) and of water (450 mL), an overall mass balance of IMD conversion into inorganic N-containing products was determined: 40±8% for NO₂, 2±0.5% for NO, 52±5% for nitrate and 16±2% for nitrite.

Table 2. Formation of NO_x after 2 h of irradiation of IMD (10⁻⁴ M) or mixtures NO₃⁻/NO₂⁻ in device 1.

Conditions	Quantity of IMD converted	Quantity of NO ₂ formed (molar yield)	Quantity of NO formed (molar yield)
IMD (10 ⁻⁴ M)	380±20 µg	24±5 µg (40±8%)	0.88±0.20 µg (2±0.5%)
NO ₃ ⁻ (1.8×10 ⁻⁶ M)			
+		1.6±0.3 µg	3.9±0.8 µg
NO ₂ ⁻ (1.7×10 ⁻⁶ M)			
NO ₃ ⁻ (2×10 ⁻⁵ M)			
+		4.8±1.0 µg	11.6±2.3 µg
NO ₂ ⁻ (5×10 ⁻⁶ M)			

As the presence of $\text{NO}_3^-/\text{NO}_2^-$ in the aqueous solution could potentially generate NO_x ³³, we irradiated these ions independently to estimate their contribution to the pool of NO_x detected upon irradiation of IMD. We chose to perform these comparative experiments with $\text{NO}_3^- = 1.8 \times 10^{-6} \text{ M}$ and $\text{NO}_2^- = 1.7 \times 10^{-6} \text{ M}$ corresponding to the concentrations estimated after 2 h of irradiation in device 1 (Figure SI-4). The irradiation of this mixture for 2 h yielded 15-fold less NO_2 and 4.4-fold more NO than the irradiation of IMD (10^{-4} M) (Table 2). The amount of NO_x formed above the IMD solution was 4.5-fold higher than that above the $\text{NO}_3^-/\text{NO}_2^-$ solution showing that IMD was the main contributor. Moreover, the higher yield of NO in the latter system confirmed that the NO_x precursor in the $\text{NO}_3^-/\text{NO}_2^-$ mixture was NO_2^- through reaction (3). At higher concentrations of $\text{NO}_3^-/\text{NO}_2^-$ ($2.0 \times 10^{-5} \text{ M}$ and $5 \times 10^{-6} \text{ M}$, respectively) not far from those reached after 16h of IMD irradiation, NO and NO_2 levels were 3-fold higher than in the previous case, respectively, showing that, in this concentration range, the NO and NO_2 amounts accumulated proportionally to NO_2^- concentration. Again, the amount of NO_x generated from NO_2^- ($2.0 \times 10^{-5} \text{ M}$) was still below the one formed upon irradiation of IMD solution.

As previously shown, the bond N-NO_2 was cleaved when IMD was irradiated in the solid phase at 305 nm and 254 nm.¹⁷ However, some questions remain unanswered: would the proposed mechanism in the solid phase and at short wavelength be still valid in solution and at longer wavelength, and thus at lower excitation energy? How is NO formed and how the oxygen atom is eliminated? In an attempt to answer these questions, we performed quantum calculations.

Theoretical Calculations. Several conformers were found for the solvated imidacloprid system. The structure of the global minimum was similar to that found from recent first-principles^{17,34} and crystallographic investigations³⁴ (see SI section for all structures reported in this work). Moreover, the DFT method used here was able to reproduce accurately the experimental absorption spectrum (see Figure 3).

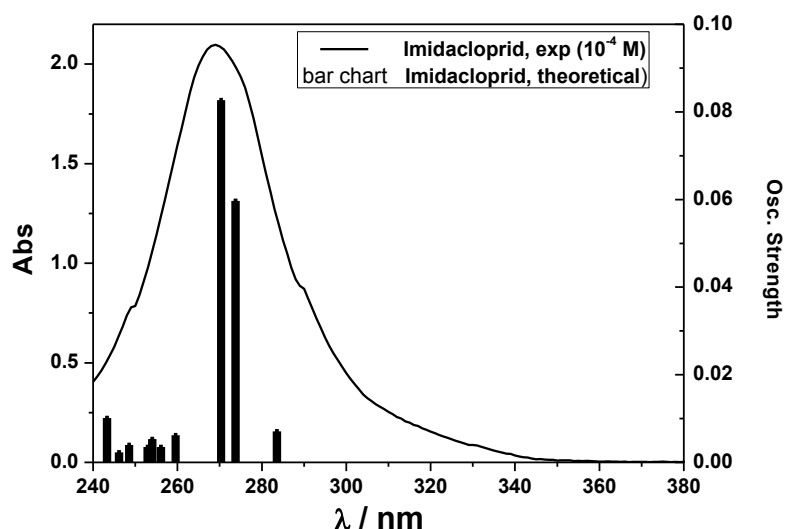


Figure 3. Experimental (Abs, left axis) and theoretical (oscillator strengths, right axis) absorption spectra of imidacloprid (theoretical spectrum for the most stable conformer (Fig. SI-5a) at the TD-MN12SX/6-311++G(d,p),PCM//MN12SX/6-31+G(d,p),PCM level. The oscillator strength is the probability of absorption. It is related to the dipole strength of the transition and is proportional to the molar absorptivity maximum for this transition. The S_1 - S_0 transition is optically active (284 nm). The oscillator strength of this transition is 0.02 which is significant (an ϵ of about $6000 \text{ L.mol}^{-1}.\text{cm}^{-1}$ can be estimated from this value when a UV-Vis Half-Width at half-height of 0.333 eV is used to model the absorption spectrum).

Detailed investigation of the ground state (S_0), first triplet state (T_1) and first singlet excited state (S_1) was performed. Some of the key results are shown in Figure 4 and discussed below.

Minima and transition state structures are given in the SI section. The dissociation pathways of interest are depicted in this Figure: NO_2 is obtained in the left-hand side of Figure 4, and triplet atomic oxygen (a reaction that is precursor to the production of NO) is shown on the right-hand side of Figure 4. The Minimum Energy Path was followed to investigate the formation of NO_2 in S_1 by performing partial optimizations of imidacloprid for fixed RN- NO_2 bond distances. The MEP maximum is indicated by a dashed level in Figure 4.

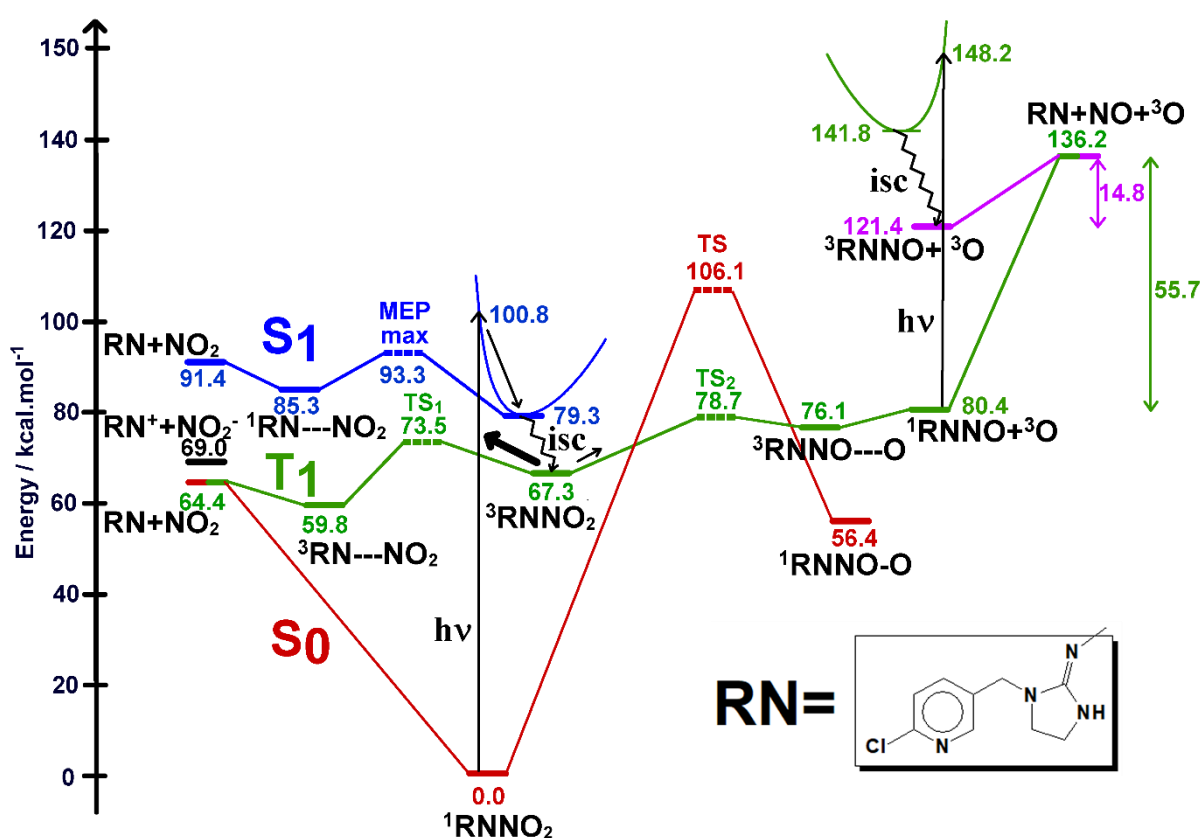


Figure 4. The electronic energies of stationary points in the ground state (S_0 , red), first triplet (T_1 , green) and first singlet (S_1 , blue) excited states of imidacloprid ($^1\text{RNNO}_2$). Calculations were performed with the MN12SX/6-311++G(d,p),PCM/MN12SX/6-31+G(d,p),PCM method. Transition states and the MEP maximum are represented with dashed levels. Dashed bonds represent long-range separations. The energies of separated fragments $\text{RN} + \text{NO}_2$ and

$^1\text{RNNO} + ^3\text{O}$ are also given in this Figure. The energy of the heterolytic dissociation products (left-hand side, black) and the triplet state of RNNO (right-hand side, purple) are also indicated. The separated fragments RN and NO_2 in S_1 are respectively in the first doublet excited state (RN) and doublet ground state (NO_2).

S_0 and S_1 states. Our results show that departure of atomic triplet oxygen is not favored in the ground state because the predissociated intermediate $^1\text{RNNO-O}$ ($\text{R(O-O)}=1.523 \text{ \AA}$; $56.4 \text{ kcal.mol}^{-1}$) cannot be reached due to very large activation energy ($106.1 \text{ kcal.mol}^{-1}$). Similarly, the formation of NO_2 is not expected in the ground state because the respective electronic dissociation energy in S_0 is large ($64.4 \text{ kcal.mol}^{-1}$; $\text{RN} + \text{NO}_2$). A transition state could not be found between imidacloprid ($^1\text{RNNO}_2$) and separated radicals in S_0 . This is expected for homolytic dissociations in the ground state. In S_1 , the dissociation of the RN-NO_2 bond required $14.0 \text{ kcal.mol}^{-1}$ (MEP maximum). In addition, the in-cage dissociation complex $^1\text{RN--NO}_2$ is less stable ($85.3 \text{ kcal.mol}^{-1}$) than the respective reactant ($79.3 \text{ kcal.mol}^{-1}$). Thus, dissociation in S_1 is less favored than that in the triplet state (an activation energy of $6.1 \text{ kcal.mol}^{-1}$ was found in T_1 and the reaction is now exothermic; see Figure 4). Moreover, our results show that the heterolytic dissociation mechanism would lead to species $\text{RN}^+/\text{NO}_2^-$ that are slightly less stable (see also SI) than the respective separated radicals (RN/NO_2). Thus, it seems reasonable to consider that it is the radicals that are eventually obtained in the liquid phase. However, considering the small energy difference between heterolytic and homolytic dissociation energies, a mixture of homolytic and heterolytic dissociation products might not be completely ruled out. Implicit solvation models underestimate the solvation free energy of small ions, the cases of the proton and hydroxide being emblematic of this issue. In order to address this point, we computed $\Delta G^*_{\text{r,calc}}$ the dissociation Gibbs free energy for both heterolytic and homolytic NO_2 cleavage. In this calculation, $RT \times \ln(24.46)$ was added to

$\Delta G^*_{r,calc}$ to account for the free energy change of 1 mol of an ideal gas from 1 atm to 1M.³⁵
 $\Delta G^0_{r,calc} = \Delta G^*_{r,calc} + RT \times \ln(24.46)$ was 58.6 and 49.2 kcal.mol⁻¹ for, respectively, the
heterolytic and homolytic dissociation reactions, thus a difference of 9.4 kcal.mol⁻¹ (recall that
the respective difference of electronic energies was smaller, i.e. 4.6 kcal.mol⁻¹). Considering
the implicit solvation model may underestimate the solvation free energy for NO₂⁻ by as much
as 10 kcal.mol⁻¹, the radical dissociated species are still more stable than the heterolytic
dissociation fragments, in agreement with our results.

Triplet State T₁. Second, S₁/T₁ intersystem-crossing (*isc*) is favored because minimum
energy geometries in S₁ and T₁ are very similar for **RNNO₂** and the energy gap is small (less
than 0.1 kcal.mol⁻¹ at the Franck-Condon geometry). In addition, in the triplet state, the barrier
for **NO₂** dissociation (6.1 kcal.mol⁻¹) is significantly smaller than that for the dissociation into
triplet atomic oxygen and singlet fragment (**¹RNNO+³O**; 11.4 kcal.mol⁻¹), in agreement with
our experimental findings. Moreover, the in-cage dissociation complex **³RNNO--O** is
thermodynamically less stable than the respective reactant **³RNNO₂** and this reaction is
displaced toward the reactant. Nevertheless, this pathway was investigated below to see if this
reaction could play a role, even minor, in the formation of NO radicals.

NO formation, a minor pathway. The mechanism for production of nitric oxide from
¹RNNO is also shown in Figure 4. NO bond dissociation energy was 55.7 kcal.mol⁻¹ for
¹RNNO in the ground state, whereas cleavage in the triplet state (reached through S₁ followed
by *isc*) required only 14.8 kcal.mol⁻¹ (**RN** is obtained). A transition state could not be found in
T₁, and the energy of activation may be identified with the dissociation energy in that case.
Thus, the formation of NO as a primary product from RNNO is probably a minor pathway.

Thus, our quantum calculations provide strong evidence that photolysis of IMD mainly leads to NO₂ formation in the overall triplet state potential energy surface while NO formation is a minor pathway.

Evidence of nitro/nitroso derivatives formation. Nitrate and nitrite ions which generate HO· radicals simultaneously with NO or NO₂ have been reported to photoinduce the nitration and/or the nitrosation of phenolic derivatives.²⁰⁻²⁴ Whether the photolysis of IMD could also contribute to the formation of such toxic products was a hypothesis that we aimed to verify in this study. Thus, IMD was irradiated with each of the three probes shown in Scheme 2 in a small reactor (device 2) for 16 h. In these conditions, the loss of IMD irradiated alone reached 60% (Figure SI-7). We first compared the probes consumption (10⁻⁴ M) in the absence and in the presence of IMD (10⁻⁴ M) to quantify the photoinductive effect (Table SI-4). The disappearance of phenol and resorcinol were drastically faster in the presence of IMD, evidencing a strong effect. Only in the case of tryptophan, the acceleration effect was small due to the fast photolysis of the probe under the studied conditions.

Then, we monitored the formation of nitro/nitroso-derivatives by UHPLC-HRMS analyses. Figure SI-8 shows the formation profile of nitroso and nitro-resorcinol upon irradiation of IMD (10⁻⁴ M) and resorcinol (10⁻⁴ M). The concentration of the two photoproducts increased linearly up to 7h of irradiation before reaching a plateau value after 16 h. Nitro and nitroso-derivatives were also detected with phenol and tryptophan. Detected levels after 16h of irradiation are given in Figure 5 (white bars) and Table SI-4. The estimated yields of nitro-resorcinols reached 3.3% of converted IMD and that of nitroso-resorcinols 5.1%. The yield of nitro-phenols (*ortho+para* derivatives)²¹ was equal to 2.6% and that of nitroso-phenols (*ortho+para* derivatives) smaller (0.5%). For tryptophan, both yields were very small,

reaching only 0.08% (nitro-derivatives) and 0.14% (nitroso-derivatives) of tryptophan converted, due to the fast direct photolysis of tryptophan.

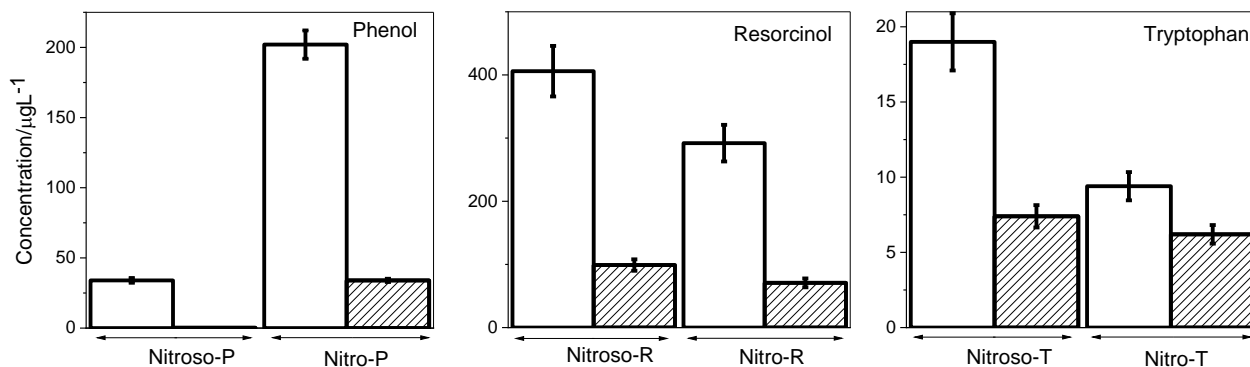


Figure 5. Concentrations of nitro and nitroso-derivatives of phenol, resorcinol and tryptophan detected after 16 h of irradiation of the probes (10^{-4} M) in device 2 in the presence of IMD (10^{-4} M) (white bars) and in presence of the mixture of NO_3^- (2×10^{-5} M) and NO_2^- (5×10^{-6} M) (shaded bars). Error bars are standard deviations.

Experiments were also performed at lower reactants concentrations to determine the impact of this parameter on the rates. A 10-fold decrease of the concentration of IMD for a concentration of resorcinol kept constant at 10^{-4} M, reduced the amount of nitro-resorcinols by 18-fold and that of nitroso-resorcinols by 9-fold while the sum of the two photoproducts was reduced by about 10-fold (Table SI-4). A 10-fold decrease of the concentration of resorcinol for a concentration of IMD kept constant at 10^{-4} M, decreased 3-fold the amount of nitro-resorcinols and 100-fold that of nitroso-resorcinols and the sum (nitro+nitroso) was reduced by about 5-fold (Table SI-4). These results indicate that the reaction rate was proportional to the concentrations of reactants. The decay rate of resorcinol followed a first order kinetic with a rate constant k that can be expressed as : $k = 5.9 \times 10^{-3} [\text{IMD}] \text{ s}^{-1}$.

We also studied the nitro/nitrosation capacity of the $\text{NO}_3^-/\text{NO}_2^-$ mixture to quantify their contributions in these reactions (shaded bars in Figure 5 and Table SI-4). For these comparisons, we fixed $\text{NO}_3^-/\text{NO}_2^-$ concentrations to those measured in the IMD solution after 16h of irradiation in device 2 (2×10^{-5} M and 5×10^{-6} M, respectively) and the mixtures $\text{NO}_3^-/\text{NO}_2^-$ + probes were irradiated for 16 h in device 2. Nitrosation was 121-fold lower in the case of phenol, 4.1-fold in the case of resorcinol and 2.6-fold in the case of tryptophan than in the presence of IMD while nitration was 5.9-fold lower for phenol, 4.1-fold for resorcinol and 1.5-fold for tryptophan. One concludes that the contributions of $\text{NO}_3^-/\text{NO}_2^-$ to the nitration/nitrosation processes observed in irradiated IMD solutions were minor especially for phenol and resorcinol even though we acknowledge that the conditions chosen for the comparative experiments (fixed $\text{NO}_3^-/\text{NO}_2^-$ concentrations) cannot perfectly reproduce the dynamic and complex evolution of $\text{NO}_3^-/\text{NO}_2^-$ during IMD irradiation.

Effect of NOM on nitration/nitrosation of probes. Another important aspect we attempted to explore is the effect of NOM on these photochemical nitration/nitrosation. Experimental conditions and results are reported in Table 3. NOM (11 mg.L^{-1}) increased the percentage of resorcinol loss in the presence of IMD by a factor of 2.6, after correction for the light screening effects (10%). The formation of nitroso and nitro-resorcinols in IMD solutions were increased by a factor of 1.3 and 2.0, respectively, and the formation of nitro and nitroso-resorcinols in NO_2^- solutions by factors of 35 and 2.8, respectively. The very low formation of nitro-resorcinols in the system NO_2^- +resorcinol was already shown.²⁰ These data highlight the significant effect of NOM on the nitro/nitroso-derivatives formation.

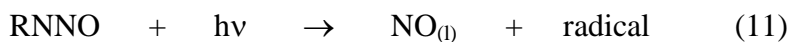
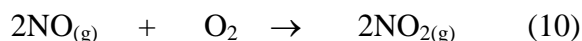
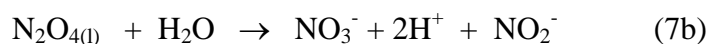
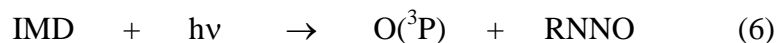
Table 3. Effect of NOM (11 mg.L⁻¹) on the photo-nitration/photo-nitrosation of resorcinol (10⁻⁴ M) after 2 h of irradiation in device 2 in the presence of IMD (10⁻⁴ M) or NO₂⁻ (5×10⁻⁶ M). The light screening effect of NOM (10%) is taken into account.

Conditions	% resorcinol converted	Nitroso- derivatives formed (μg.L ⁻¹)	Nitro- derivatives formed (μg.L ⁻¹)
IMD +resorcinol	7.0±0.3	83±8	44±4
IMD +resorcinol+NOM	18±1	110±10	88±9
NO₂⁻ +resorcinol	< 1	20±2	1±0.1
NO₂⁻ +resorcinol+NOM	< 1	55±5	35±3

Reaction mechanism. Many reactions are expected to take place in this complex system. The main ones are summarized below. The photolysis of IMD in water generates NO₂ in the liquid phase (NO_{2(l)}) together with the radical RN as shown by the quantum calculations and this latter gives rise mainly to desnitro-IMD (reaction 5). The radicals O(³P) and RNNO are also produced but in much lower amounts (reaction 6). The reactivity of NO₂ in water is very high. It is reported in the literature that NO₃⁻ and NO₂⁻ are generated according reactions (7a and 7b) through the intermediary dimerisation of NO_{2(l)}.^{36,37} NO₃⁻ and NO (NO_(l)) can also be produced through reaction (8).^{37,38} In our experiments, N₂O_{4(g)} cannot be distinguished from

NO_{2(g)}. Reaction (8) is probably the major NO formation pathway, but the photolysis of RNNO (reaction 11), of NO_{2(g)} (reaction 12) and of NO₂⁻ (reaction 3) are alternative pathways for NO formation. NO is stable in water and volatilizes in the gaseous phase (reaction 9).³⁷ It generates NO_{2(g)} by reaction with oxygen (reaction 10).

In this scheme, we did not take into account the oxidation of IMD by HO[•] formed in reaction (3) because the formation of oxidation products (IMD+O) was small. NO₂⁻ and NO₃⁻ could be also oxidized by HO[•].³⁹ However, due to the high concentration of IMD compared to those of NO₂⁻ and NO₃⁻ in the first half of the reaction, IMD and its main photoproduct desnitro-IMD are expected to be the main sinks of HO[•].



The nitration/nitrosation of phenolic/aromatic compounds in the presence of NO₂⁻ or NO₃⁻ has been already studied.^{20-25,39-41} NO₂ is recognized as having a key role in these reactions, even though the mechanisms are not fully understood. Several studies attributed the formation of phenoxyl radicals to the reaction of phenols with NO₂^{20,25,39,41} while others to their reaction

with HO[•].⁴⁰ Once formed phenoxyl radicals further react NO₂ to yield the ortho and para derivatives of nitro-phenols. Similarly, the reaction of phenoxyl radicals with NO are expected to generate nitroso-phenols. The effect of NOM on these reactions is difficult to predict due to the existence of opposite reactions. Indeed, on the first hand, NOM can potentially favor nitro/nitrosation reactions by generating photooxidants such as triplet excited states (³NOM*), singlet oxygen or HO[•] that are expected to induce the formation of phenoxyl radicals as shown in the literature.³⁹ In addition, ³NOM* or HO[•] could be able to oxidize NO₂⁻ and NO₃⁻ into NOx³⁹ (see process 13 related to NO₂⁻):



On the other hand, NOM could be also a sink for NOx due to the presence of aromatic moieties in its structure and therefore could inhibit the nitration/nitrosation reaction to some extent.^{26,42} The overall effect of NOM will thus depend on the experimental conditions and in particular on the relative concentrations of reactants. In our set-up, the presence of NOM (11 mg.L⁻¹) in IMD or NO₂⁻ solutions containing resorcinol (10⁻⁴ M) increased the amounts of nitro and nitroso-resorcinols showing that in this case NOM favors the formation of the phenoxyl radical and of NO₂. Since Suwannee River NOM contains 68% of fulvic acids and fulvic acids contain ~3 mmol oxidizable phenol per g of carbon⁴³, there are about 20 μM of oxidizable phenols originating from NOM in a solution containing 11 mg/l. Under these conditions where the quenching molecule is in large excess over phenolic moieties in NOM, it can be expected that the majority of NOM-derived photooxidants will be quenched by the probe compounds to form phenoxyl radicals, which can then further react with NOx to produce nitro/nitroso-phenol/resorcinol, enhancing the yields of these products as it is observed.

428

429 **Environmental significance.** Our study showed that NO_x (NO and NO₂) could be generated
430 by irradiation of IMD and that these NO_x were capable of reacting with phenolic probes to
431 produce nitro and nitroso-derivatives. This suggests that in surface water, IMD could induce
432 the formation of nitro and nitroso derivatives of other contaminants that could be toxicants in
433 the aquatic environment. The importance of the phenomenon will depend on the level of IMD
434 present in surface waters. The frequency of IMD detection in surface waters is high and
435 concentration of IMD varies in a large range reaching 1 µg.L⁻¹ in agricultural areas.^{3,4} Based
436 on this work and on the light absorption capacities of IMD and NO₂⁻, one can calculate that at
437 1 µg.L⁻¹, IMD could generate as much as nitroso/nitro-derivatives as NO₂⁻ at 0.1 µg.L⁻¹. The
438 relative contributions of NO₂⁻ and IMD to nitroso/nitro-derivatives formation depend
439 therefore on their levels in water. NO₂⁻ is present in surface waters at a maximal concentration
440 of 0.1 mg.L⁻¹.⁴⁴ In many cases, NO₂⁻ concentration will be high enough to make negligible
441 the contribution of IMD in nitro/nitrosation reactions. However, in waters containing very low
442 levels of NO₂⁻ and high levels of IMD, IMD might play a role in the nitro/nitrosation
443 reactions.

444 On the other hand, we observed that NOM (11 mg.L⁻¹) enhanced nitro and nitrosation
445 reactions of phenols (10⁻⁴ M). The yield of nitro-resorcinol was multiplied by 2 whereas that
446 of nitroso-resorcinol by 1.3 and when NO₂⁻ was used instead of IMD, the yields of nitro-
447 resorcinol and of nitroso-resorcinol were 35-fold and 2.8-fold increased respectively. This can
448 be explained by the enhanced formation of phenoxyl radicals in the quenching of NOM
449 deriving photooxidants by phenols. However, this effect might be concentration-dependent.
450 The level of NOM used in this study falls in the range of typical NOM levels found in rivers
451 and eutrophic lakes⁴⁵, but those of probes are high. At environmentally relevant
452 concentrations of the probe compounds (<1 µM), phenolic moieties in NOM are in excess and

it might be possible that the NOM-bound phenoxyl radicals, in higher concentration than probe -derived phenoxyl radicals might outcompete the latter for reaction with NO_x. In other words, at environmentally relevant conditions, a shift towards nitration/nitrosation of NOM seems possible and the yield of nitro/nitroso-derivatives of probes could then be lower compared to the ones in the absence of NOM. The incorporation of N inorganic nitrogen (N) into NOM *via* photolysis of nitrate/nitrite and/or in advanced oxidation processes treatments was already reported and shown to generate also potentially toxic compounds.²⁶⁻²⁸ Therefore such reactions might have also environmentally negative consequences. We could not detect any significant structural changes in NOM using HRMS analyses. Nevertheless, further experiments using N-labelled IMD or nitrite/nitrate and other hyphenated techniques may provide evidence of NOM nitration/nitrosation. Therefore, a consistent monitoring of nitro/nitroso byproducts is highly recommended to verify their potential formation.

Our study confirms the capacity of water contaminants to interact with each other under irradiation and to induce mutual degradation. Mutual effects can involve reactions between excited and ground states contaminants or the intermediary formation of reactive species like NO_x in the case of IMD. Up to now, they have been poorly investigated in photochemical studies and would deserve more attention. Thus, future studies should further consider the investigation of the “cocktail effect” on the environmental fate of contaminants and more specifically the reactivity of intermediates in order to enable a more reliable monitoring of non-target pollutants and assessment of potential risks.

ASSOCIATED CONTENTS

Supporting information:

15 pages, 8 Figures and 4 Tables

Spectrum of light received by the solutions in devices 1 and 2. NO_x formation in device 1 upon photolysis of IMD (10⁻⁴ M). Calibration curve for nitroso-phenol and for nitro-phenol. Profile of NO_x, NO₃⁻, NO₂⁻, nitroso-resorcinol and nitro-resorcinol formations and of IMD consumption. Structure and cartesian coordinates of the minimum energy structures of IMD in S₀ (a), S₁ (b) and T₁ (c), the TS (d), intermediate RNNO-O (e) in S₀, TS₁ in T₁ (f), TS₂ in T₁ (g), ³RN-NO₂ (h), ³RN-NO₂ in T₁ (i), ¹RNNO (j) and ³RNNO (k) at the B3LYP/6-311++G(d,p)//B3LYP/6-31+G(d,p) level. Minima and transition state structures with cartesian coordinates. Photo-nitration and photo-nitrosation of the probes after 16 h of irradiation in presence of IMD (10⁻⁵ or 10⁻⁴ M) or a mixture of NO₃⁻ (2×10⁻⁵ M) and NO₂⁻ (5×10⁻⁶ M). Effect of NOM (11 mg L⁻¹) on the photo-nitration/photo-nitrosation of resorcinol (10⁻⁴ M) after 2 h of irradiation in device 2 in the presence of IMD (10⁻⁴ M) or NO₂⁻ (5×10⁻⁶ M).

ACKNOWLEDGEMENTS

This paper is part of a project that has received funding from the European Union's Horizon 2020 research and innovation programme under the Marie Skłodowska-Curie grant agreement No 765860 (Aquality). The authors also thank the European Regional Development Fund of the European Union and the Région Auvergne-Rhône-Alpes for financial support under the Program "Nouveau Chercheur" (N° AV0004494) which allowed the acquisition of NO_x analyzer. We thank Martin Leremboure and Guillaume Vyard (CNRS engineers), for assistance with chromatographic and mass spectrometry analyses and the anonymous reviewers who helped to improve the manuscript.

500 Disclaimer: The paper reflects only the author's view and that the Agency is not responsible
501 for any use that may be made of the information it contains.

502

503

REFERENCES

- 1- Jeschke, P.; Nauen, R.; Schindler, M.; Elbert, A. Overview of the status and global strategy for neonicotinoids. *J. Agric. Food Chem.* **2011**, *59* (7), 2897–2908. DOI:10.1021/jf101303g

- 2- Désert, M. ; Ravier, S. ; Gill, G. ; Quinapallo, A. ; Armengaud, A. ; Pochet, G. ; Savelli, J.L. ; Wortham, H. ; Quivet, E. Spatial and temporal distribution of current-use pesticides in ambient air of Provence-Alpes-Côte-d’Azur Region and Corsica, France. *Atmos. Environ.* **2018**, *192*, 241-256. DOI:10.1016/j.atmosenv.2018.08.054

- 3- Struger, J. ; Grabuski, J. ; Cagampan, S. ; Sverko, E. ; Mcgoldrick, D. ; Marvin, C. H. Factors influencing the occurrence and distribution of neonicotinoid insecticides in surface waters of southern Ontario, Canada. *Chemosphere* **2017**, *169*, 516-523. DOI:10.1016/j.chemosphere.2016.11.036

- 4- Hladik, M. L.; Kolpin, D. W.; Kuivila, K. M. Widespread occurrence of neonicotinoid insecticides in streams in a high corn and soybean producing region, USA. *Environ. Pollut.* **2014**, *193*, 189-196. DOI:10.1016/j.envpol.2014.06.033

- 5- Abou-Donia, M.B. ; Goldstein, L.B. ; Bullman, S. ; Tu, T. ; Khan, W.A. ; Dechkovskaia, A.M. ; Abdel-Rahman, A.A. Imidacloprid induces neurobehavioral deficits and increases expression of glial fibrillary acidic protein in the motor cortex and hippocampus in offspring rats following in utero exposure. *J. Toxicol. Environ. Health. A.* **2008**, *71*, 119-130. DOI:10.1080/15287390701613140

525 6- Laycock, I. ; Lenthall, K. M. ; Barratt, A. T. ; Cresswell, J. E. Effects of imidacloprid, a
526 neonicotenoid insecticide, on reproduction in worker bumble bees (*Bombus terrestris*)
527 *Ecotoxicol.* **2012**, *21*(7), 1937-1945. DOI:10.1007/s10646-012-0927-y
528

529 7- Woodcock, B.A. ; Isaac, N.J. ; Bullock, J.M. ; Roy, D.B. ; Garthwaite, D.G. ; Crowe, ;
530 Pywell R.F. Impacts of neonicotinoid use on long-term population changes in wild bees in
531 England *Nat. Commun.* **2016**, *7*, 12459. DOI:10.1038/ncomms12459

532 8- Berheim, E. H. ; Jenks, J. ; Lundgren, J. G. ; Michel, E. S. ; Grove, D. ; Jensen, W. F.
533 Effects of neonicotenoid insecticides on physiology and reproductive characteristics of
534 captive female and fawn white-tailed deer. *Sci. Rep.* **2019** *9*, 1-10. DOI:10.1038/s41598-019-
535 40994-9
536

537 9- Vesile, D. ; Suat E. Acute oxidant and inflammatory effects of imidacloprid on the
538 mammalian central nervous system. *Pestic. Biochem. Physiol.* **2010**, *97*, 13-18.
539 DOI:10.1016/j.pestbp.2009.11.008
540

541 10- Moza, P. N.; Hustert, K.; Feicht, E.; Kettrup, A. Photolysis of imidacloprid in aqueous
542 solution. *Chemosphere* **1998**, *36*(3), 497-502. DOI:10.1016/S0045-6535(97)00359-7

543 11- Redlich, D.; Shahin, N.; Ekici, P.; Friess, A.; Parlar, H. Kinetical study of the
544 photoinduced degradation of imidacloprid in aquatic media. *Clean: Soil, Air, Water* **2007**,
545 *35*(5), 452–458. DOI:10.1002/clen.200720014

- 546 12- Wamhoff, H.; Schneider, V. Photodegradation of imidacloprid. *J. Agric. Food Chem.*
547 **1999**, 47(4), 1730–1734. DOI:10.1021/JF980820J
- 548 13- Zheng, W.; Liu, W.P.; Wen, Y.Z.; Lee, S.-J. Photochemistry of insecticide imidacloprid:
549 direct and sensitized photolysis in aqueous medium. *J. Environ. Sci.* **2004**, 16(4), 539–542.
550 Journal Code:100967627 Netherlands
- 551 14- Schippers, N.; Schwack, W. Photochemistry of imidacloprid in model systems. *J. Agric.*
552 *Food Chem.* **2008**, 56 (17), 8023–8029. DOI:10.1021/jf801251u
- 553 15- Scholz, K.; Reinhard, F. Photolysis of imidacloprid (NTN33893) on the leaf surface of
554 tomato plants. *Pestic. Sci.* **1999**, 55(6), 652–654. DOI:10.1002/(SICI)1096-
555 9063(199906)55:6<652::AID-PS997>3.0.CO;2-I
- 556 16- Schippers, N.; Schwack, W. Phototransformation of imidacloprid on isolated tomato fruit
557 cuticles and on tomato fruits. *J.Photochem. Photobiol. B* **2010**, 98(1), 57–60.
558 doi.org/10.1016/j.jphotobiol.2009.11.004
- 559 17- Aregahegn, K. Z. ; Shemesh, D. ; Gerber, R. B. ; Finlayson-Pitts, B. J. Photochemistry of
560 thin solid films of the neonicotinoid imidacloprid on surfaces. *Environ. Sci. Technol.* **2017**,
561 51(5), 2660–2668. doi.org/10.1021/acs.est.6b04842
562
- 563 18- Monadjemi, S.; Richard, C. Accelerated dissipation of the herbicide cycloxydim on wax
564 films in the presence of the fungicide chlorothalonil and under the action of solar light. *J.*
565 *Agric. Food Chem.* **2014**, 62(21), 4846–4851. DOI:10.1021/jf500771s

566 19- Kouras-Hadef, S.; Hamdache, S.; Sleiman, M.; de Sainte-Claire, P.; Richard, C.
567 Photodegradation of the fungicide Thiophanate-methyl into a sensitizing photoproduct.
568 *J.Photochem. Photobiol. A* **2018**, *360* (1), 262-269. DOI:10.1016/j.jphotochem.2018.04.046

569 20- Machado, F.; Boule, P. Photonitration and photonitrosation of phenolic derivatives
570 induced in aqueous solution by excitation of nitrite and nitrate ions. *J. Photochem. Photobiol.*
571 *A: Chem.* **1995**, *86*(1-3), 73-80. DOI:10.1016/1010-6030(94)03946-R

572 21- Vione, D.; Maurino, V.; Pelizzetti, E.; Minero, C.. Phenol Photonitration and
573 Photonitrosation upon Nitrite Photolysis in basic solution. *Int. J. Environ. Anal. Chem.*
574 **2004**, *84*(6-7), 493-504. DOI:10.1080/03067310310001640447

575 22- Suzuki, J.; Yagi, N.; Suzuki, S. Photochemical nitrosation of phenol in aqueous nitrite
576 solution. *Chem. Pharm.Bull.* **1984**, *32*(7), 2803-8. DOI:10.1248/cpb.32.2803

577 23- De Laurentiis, E.; Minella, M.; Berto, S.; Maurino, V.; Minero, C.; Vione, D. The fate of
578 nitrogen upon nitrite irradiation: Formation of dissolved vs. gas-phase species. *J. Photochem.*
579 *Photobiol. A: Chem.* **2015**, *307-308*, 30-34. DOI:10.1016/j.jphotochem.2015.04.005

580 24- Scholes, R. C.; Prasse, C.; Sedlak, D. L. The Role of Reactive Nitrogen Species in
581 Sensitized Photolysis of Wastewater-Derived Trace Organic Contaminants. *Environ. Sci.*
582 *Technol.* **2019**, *53* , 6483-6491. DOI:10.1021/acs.est.9b01386

583 25- Vione, D.; Maurino, V.; Minero, C.; Pelizzetti, E. New processes in the environmental
584 chemistry of nitrite: nitration of phenol upon nitrite photoinduced oxidation. *Environ. Sci.*
585 *Technol.* **2002**, *36*, 15, 669-676. DOI:10.1021/es010101c

586 26- Thorn, K. A.; Cox, L. G. Ultraviolet irradiation effects incorporation of nitrate and nitrite
587 nitrogen into aquatic natural organic matter. *J. Environ. Qual.* **2012**, *41*(3), 865-881.
588 DOI:10.2134/jeq2011.0335

589 27- Yang, P.; Ji, Y.; Lu, J.; Huang, Q. Formation of nitrophenolic byproducts during heat-
590 activated peroxydisulfate oxidation in the presence of natural organic matter and nitrite.
591 *Environ. Sci. Technol.* **2019**, *53*, 4255-4264. DOI:10.1021/acs.est.8b06967

592 28- Ji, Y.; Wang, L.; Jiang, M., Lu, J.; Ferronato, C. ; Chovelon, J.-M. The role of nitrite in
593 sulfate radical-based degradation of phenolic compounds: An unexpected nitration process
594 relevant to groundwater remediation by in-situ chemical oxidation (ISCO). *Water Res.* **2017**,
595 *123*, 249-257. DOI:10.1016/j.watres.2017.06.081

596 29- Kieber, R. J.; Seaton, P. J. Determination of Subnanomolar Concentrations of Nitrite in
597 Natural Waters. *Anal. Chem.* **1995**, *67*(18), 3261-4. DOI:10.1021/ac00114a024
598

599 30- Gaussian 09, *Revision C.01*, Frisch, M. J. ; Trucks, G. W. ; Schlegel, H. B. ; Scuseria, G.
600 E. ; Robb, M. A. ; Cheeseman, J. R. ; Scalmani, G. ; Barone, V. ; Mennucci, B. ; Petersson, G.
601 A. ; Nakatsuji, H. ; Caricato, M. ; Li, X. ; Hratchian, H. P. ; Izmaylov, A. F. ; Bloino, J. ;
602 Zheng, G. ; Sonnenberg, J. L. ; Hada, M. ; Ehara, M. ; Toyota, K. ; Fukuda, R. ; Hasegawa,
603 J. ; Ishida, M. ; Nakajima, T. ; Honda, Y. ; Kitao, O. ; Nakai, H. ; Vreven, T. ; Montgomery

604 Jr., J. A. ; Peralta, J. E. ; Ogliaro, F. ; Bearpark, M. ; Heyd, J. J. ; Brothers, E. ; Kudin, K. N. ;
 605 Staroverov, V. N. ; Keith, T. ; Kobayashi, R. ; Normand, J. ; Raghavachari, K. ; Rendell, A. ;
 606 Burant, J. C. ; Iyengar, S. S. ; Tomasi, J. ; Cossi, M. ; Rega, N. ; Millam, J. M. ; Klene, M. ; K
 607 nox, J. E. ; Cross, J. B. ; Bakken, V. ; Adamo, C. ; Jaramillo, J. ; Gomperts, R. ; Stratmann, R.
 608 E. ; Yazyev, O. ; Austin, A. J. ; Cammi, R. ; Pomelli, C. ; Ochterski, J. W. ; Martin, R. L. ;
 609 Morokuma, K. ; Zakrzewski, V. G. ; Voth, G. A. ; Salvador, P. ; Dannenberg, J. J. ; Dapprich,
 610 S. ; Daniels, A. D. ; Farkas, O. ; Foresman, J. B. ; Ortiz, J. V. ; Cioslowski, J. ; Fox, D. J.
 611 Gaussian, Inc., Wallingford CT, **2010**.
 612
 613 31- Peverati R.; Truhlar, D. G. Screened-exchange density functionals with broad accuracy
 614 for chemistry and solid state physics. *Phys. Chem. Chem. Phys.* **2012**, *14*, 16187-16191.
 615 DOI:10.1039/C2CP42576A
 616
 617 32- Vione, D. ; Maurino, V. ; Minero, C.; Pelizzetti , E. Reactions induced in natural waters
 618 by irradiation of nitrate and nitrite ions. *Hdb. Env. Chem.* Vol 2, Part M, Springer-Verlag
 Berlin (**2005**) pp 221-253.
 619
 620 33- Richards-Henderson, N. K.; Anderson, C.; Anastasio, C.; Finlayson-Pitts, B. J. The effect
 621 of cations on NO₂ production from the photolysis of aqueous thin water films of nitrate salts.
 622 *Phys. Chem. Chem. Phys.* **2015**, *17*(48), 32211-32218. DOI:10.1039/C5CP05325K
 623
 624 34- Le Questel, J.-Y.; Graton, J.; Cerón-Carrasco, J. P.; Jacquemin, D.; Planchat, A.; Thany,
 625 S. H. New insights on the molecular features and electrophysiological properties of
 626 dinotefuran, imidacloprid and acetamiprid neonicotinoid insecticides. *Bioorg. Med. Chem.*
2011, *19*, 7623–7634. DOI:10.1016/j.bmc.2011.10.019

627 35- Bryantsev, V. S.; Diallo, M. S.; Goddard, W. A., III Calculation of Solvation Free
 628 Energies of Charged Solutes Using Mixed Cluster/Continuum Models. *J. Phys. Chem. B*
 629 **2008**, *112*, 9709–9719. DOI: 10.1021/jp802665d
 630

631 36- Grätzel, M. ; Henglein, A ; Lilie, J. ; Beck, G. Pulsradiolytische untersuchung einiger
 632 elementarprozesse der oxydation und reduktion des nitritions. *Ber. Bunsenges. Phys. Chem.*
 633 **1968**, *73* ,646-653. DOI : 10.1002/bbpc.19690730707
 634

635 37- Tan, S.P.; Piri, M. Modeling the solubility of nitrogen dioxide,in water using perturbed-
 636 chain statistical associating fluid theory. *Ind. Eng. Chem. Res.* **2013**, *52*, 16032-16043.
 637 DOI:10.1021/ie402417p

638 38- Burdick, C. L.; Freed, E. S. The equilibrium between nitric oxide, nitrogen peroxide and
 639 aqueous solution of nitric acid. *J. Am. Chem. Soc.* **1921**, *43*, 518-530.
 640 DOI:10.1021/ja01436a015
 641

642 39- Vione, D ; Minella, M. ; Maurino, V. ; Minero C. Indirect Photochemistry in Sunlit
 643 Surface Waters: Photoinduced Production of Reactive Transient Species. *Chem. Eur. J.* **2014**,
 644 *20*, 10590-10606. DOI : 10.1002/chem.201400413
 645

646 40- Barzaghi, P.; Herrmann, H. A mechanistic study of the oxidation of phenol by
 647 OH/NO₂/NO₃ in aqueous solution. *Phys. Chem. Chem. Phys.* **2002**, *4*, 3669-3675.
 648 DOI:10.1039/b201652d

- 649 41- Alfassi, Z. B.; Huie, R. E.; Neta, P. Substituent effects on rates of one-electron oxidation
650 of phenols by the radicals ClO_2 , NO_2 , SO_3^- . *J. Phys. Chem.* **1986**, *90*, 4156-4158.
651 DOI:10.1021/j100408a063
- 652 42- Semitsoglou-Tsiapou, S.; Templeton, M.R.; Graham, N.J.D.; Mandal, S.; Hernández Leal,
653 L.; Kruithof, J.C. Potential formation of mutagenicity by low pressure-UV/ H_2O_2 during the
654 treatment of nitrate-rich source waters. *Environ. Sci.: Wat. Res. Technol.* **2018**, *4* (9), 1252-
655 1261. DOI:10.1039/C7EW00389G
- 656 43- Ma, H. ; Allen, H. ; Yin, Y. Characterization of isolated fractions of dissolved organic
657 matter from natural waters and a wastewater effluent. *Wat. Res.* **2001**, *35*, 985-996.
658 DOI:10.1016/s0043-1354(00)00350-x
659
- 660 44- Keeney, D. ; Olson, R. A. Sources of nitrate to ground water. *Crit. Rev. Environ. Control.*
661 **1986**, *16*, 257-304. DOI :10.1080/10643388609381748
662
- 663 45- Perdue, E. M. Natural organic matter in « Biogeochemistry of Inland waters », G. E.
664 Likens (ed), Academic Press, **2009**. pp 503-516.

665
666
667
668